Photonic band gap phenomenon and optical properties of artificial opals

V. N. Bogomolov
A. F. Ioffe Physico-Technical Institute, Russian Academy of Sciences, Politekhnicheskaya Street 26, St. Petersburg 194021, Russia

S. V. Gaponenko, I. N. Germanenko, A. M. Kapitonov, and E. P. Petrov
B. I. Stepanov Institute of Physics, Academy of Sciences of Belarus, F. Skaryna Avenue 70, Minsk 220072, Belarus

N. V. Gaponenko
Belarusian State University of Informatics and Radioelectronics, P. Brovka Street 6, Minsk 220600, Belarus

A. V. Prokofiev
A. F. Ioffe Physico-Technical Institute, Russian Academy of Sciences, Politekhnicheskaya Street 26, St. Petersburg 194021, Russia

A. N. Ponyavina and N. I. Silvanovich
Institute of Molecular and Atomic Physics, Academy of Sciences of Belarus, F. Skaryna Avenue 68, Minsk 220072, Belarus

S. M. Samoilovich
M. V. Lomonosov Moscow State University, Moscow 117234, Russia

(Received 18 July 1996; revised manuscript received 19 December 1996)

We report on the photonic band gap phenomenon in the visible range in a three-dimensional dielectric lattice formed by close-packed spherical silica clusters. The spectral position and the spectral width of the optical stop band depend on the direction of light propagation with respect to the crystal axes of opal, and on the relative cluster-to-cavity refraction index n. Manifestations of the photonic pseudogap have been established for both transmission and emission spectra. The stop band peak wavelength shows a linear dependence on n. Transmission characteristics of the lattice have been successfully simulated by numerical calculations within the framework of a quasicrystalline approximation. [S1063-651X(97)13805-3]

PACS number(s): 42.70.Qs, 42.25.−p, 42.65.−k

I. INTRODUCTION

The concept of the photonic crystal that behaves with respect to photon waves like a dielectric crystal does with respect to electron waves has been advanced by Yablonovitch [1] and John [2], and stimulated extensive studies in this field [3]. A number of basic issues like the photon effective mass, Anderson localization of photons, modification of the photon density of states, inhibition and enchancement of spontaneous emission, coupled atom-field states, and others are currently being discussed in relation to three-dimensional dielectric lattices [4–6]. In spite of significant progress in theoretical analysis of these problems, experimental studies are still rather fragmentary. The photonic band gap has been observed in the radio frequency range [7,8], whereas the main field of application of the new class of phenomena is expected to be optical and laser physics. Experiments in the optical range have been carried out for one-dimensional lattices (see Ref. [9], and references therein) in which the effect of spatial arrangement on photon localization and the spontaneous emission rate has been observed. A breakthrough toward actual photonic crystals with the forbidden frequency gap in the optical range has been made using ordered ensembles of highly monodisperse polystyrene particles [10]. These microstructures form colloidal cubic crystals, which were found to affect the spontaneous emission of organic molecules [11]. Polystyrene colloidal crystals exhibit a pronounced pseudogap in the photon density of states [12].

The pseudogap manifests itself as a stop band in the transmission (reflection) spectrum of a refractive medium with negligible dissipative losses. Stop bands arise due to diffraction of an optical wave on a three-dimensional lattice made of dielectric particles.

For further progress toward photonic crystals possessing a real gap in all directions, it is reasonable to search for relevant solid-state structures providing a controllable variation of modulated dielectric function. Gem opals are known to consist of spatially arranged silica microspheres organized either in cubic or hexagonal lattices [13]. Whereas iridescent properties of natural and artificial opals are attributed to optical interference, to our knowledge the optical properties of opals have not been considered to date in the context of the photonic band gap phenomenon.

In the present paper we report on the photonic band gap phenomenon in solid-state opal matrices. These matrices are made of close-packed SiO_2 spherical clusters arranged in a face-centered-cubic (fcc) lattice. In Sec. II we describe results of experimental studies, including both transmission properties of the lattice formed by SiO_2 spheres, and the lattice formed by voids filled with various liquids with the refractive index higher than that of SiO_2 spheres, and properties of fluorescence of dye molecules embedded in opal samples. In Sec. III we perform numerical simulations of transmission and reflection of a three-dimensional lattice, using a quasicrystal model to calculate coherent transmission and reflection of a multilayer scattering medium with dense

 © 1997 The American Physical Society

FIG. 1. A set of opal samples with axes oriented at different angles with respect to the incident light direction (in water).

packing of particles. Section IV contains conclusions, and some considerations of further investigations in both optics and optoelectronics for three-dimensional (3D) arrays of nanostructures, as well as media that are intermediate in their properties between substances with discrete and continuous structures.

II. EXPERIMENT

We used the standard technology for the fabrication of artificial opals [14,15] to develop three-dimensional dielectric lattices. Synthetic opals are produced from a sol of artificially grown monodisperse spherical SiO_2 particles. The regular structure, obtained after precipitation of the particles, is mechanically fragile due to weak bonding between silica globules. The opals are hardened by hydrothermal treatment and annealing, and point contacts between the globules are converted into faceted ones. Under certain conditions, voids of the structure form a regular sublattice that can be filled with liquids or solid inclusions. A photograph of opal samples impregnated with water is shown in Fig. 1. Structures fabricated in such a manner consist of nearly spherical silica clusters of size ranging from 0.2 to 0.3 μm, arranged in a fcc lattice which is evident from the electron microscopy image presented in Fig. 2.

Each silica particle in its turn has an internal substructure [16] which is known also for silica gels. As a result of the presence of an internal structure, the effective refraction index $n^*_{SiO_2}$ of silica particles varies [14] from the value $n_{SiO_2}=1.45$ inherent in bulk silica down to $n^*_{SiO_2}=1.26$.

All the lattices studied show a dip in the optical transmission spectrum, with the spectral position depending on the lattice period a_L and the $n^*_{SiO_2}$ value. The nature of the spectrally selective transmission of a disperse medium with vanishing dissipation is nothing else but multiple scattering and the interference of light waves. This can be intuitively understood in terms of the Bragg diffraction of optical waves. In other words, formation of a pronounced stop band is indicative of a reduced density of photon states within the sample, and thus can by classified as a photonic pseudogap phenomenon.

Intersphere voids in the opal form a network in which cavities of two kinds and channels can be distinguished [17]. The voids can be filled with materials having a refraction

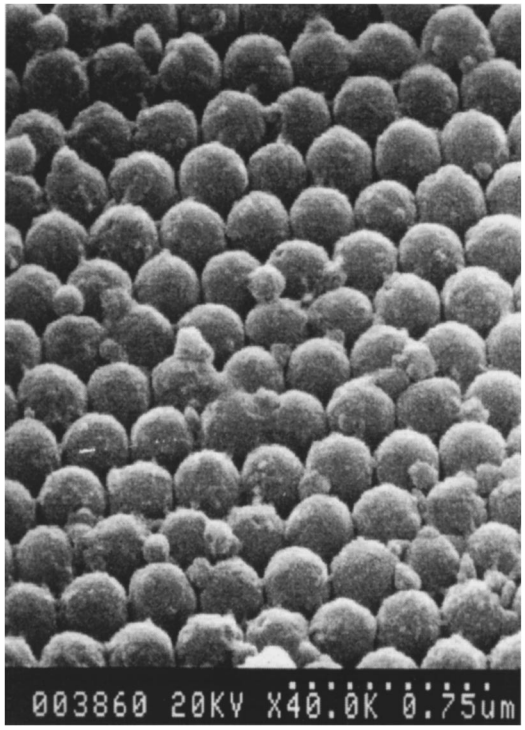

FIG. 2. Microphotograph of the opal surface.

index different than that of the spheres. Thus it is possible to control the spectral position and contrast of the stop band. Optical transmission spectra of one and the same opal matrix filled with various liquids [methanol ($n=1.328$), ethanol ($n=1.361$), cyclohexane ($n=1.426$), and toluene ($n=1.497$)] are presented in Fig. 3 (the values of the refraction index are taken from Ref. [18]). The stop band position shifts linearly toward longer wavelengths with increasing refraction index of voids relative to that of the spheres (Fig. 4).

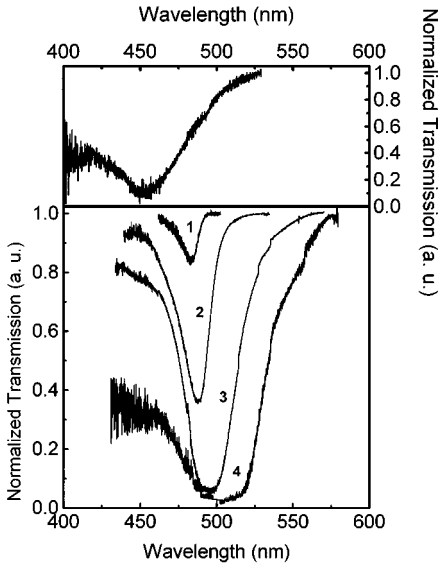

FIG. 3. Optical transmission spectra of the same sample with empty voids (upper panel) and impregnated with various fillers (lower panel): methanol (1), $n=1.328$; ethanol (2), $n=1.361$; cyclohexane (3), $n=1.426$; and toluene (4), $n=1.497$.

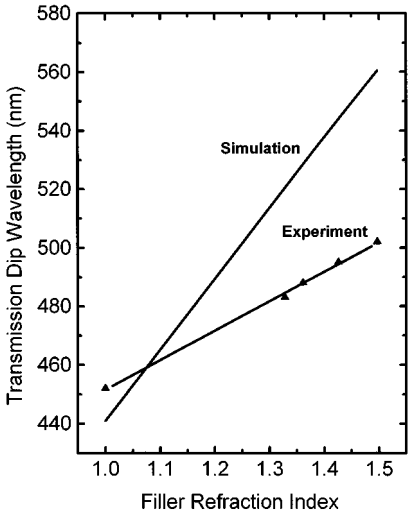

FIG. 4. Stop band peak dependence on the refraction index of the filler (calculated and measured).

Experimentally measured positions of the stop band for a dry sample ($n_{\text{voids}} < n_{\text{spheres}}$) and the same sample impregnated with liquids ($n_{\text{voids}} > n_{\text{spheres}}$) fit the common straight line well. This is probably a manifestation of the behavior known from optics of scattering media: properties of scattering on two spatially complementary ensembles of particles, e.g., dense spheres in empty space and hollow spherical voids in a dense medium, are essentially equivalent. The dip in the transmission spectrum deepens and widens with an increasing value of $n_{\text{voids}}/n_{\text{spheres}}$. The maximum transmission contrast reached in our experiments was about 10^2, the spectral width in this case was 40 nm at the 10% level (curve 4 in Fig.3).

The position of the stop band also depends on the angle between the direction of propagation of light and the crystal axes. The first Brillouin zone of a fcc lattice is shown in Fig. 5(a). The solid line in Fig. 5(b) presents an isometric projection of a real-space fcc cell on the (111) plane. The dashed line connects points with equal values of angles of deviation from $\langle 111 \rangle$ for directions corresponding to special points of

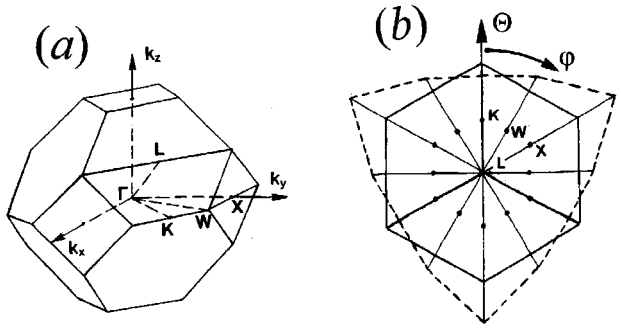

FIG. 5. (a) The first Brillouin zone of the fcc structure. (b) Isometric projection of a real-space fcc unit cell on the (111) plane (solid line); the dashed line connects points with equal values of angles of deviation from $\langle 111 \rangle$ for directions corresponding to the marked special points of the Brillouin zone. The angle Θ is the measure of deviation from $\langle 111 \rangle$, and φ is the polar angle of projection.

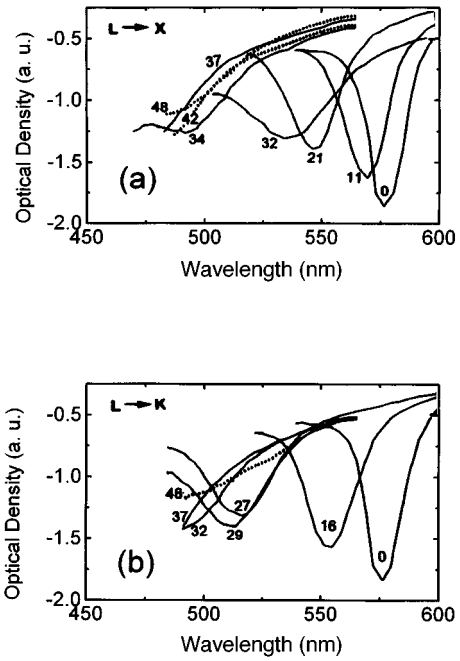

FIG. 6. Transmission spectra of the opal plate sample cut parallel to (111) filled with water for various directions of light propagation. The sample was deviated by the angle Θ in the range from 0° to 48° such as to correspond to (a) (ΓLX) and (b) (ΓLK) planes. Numbers at the curves indicate the angle Θ value.

the Brillouin zone. In order to follow the direction of propagation of light, we can introduce two angles Θ and φ. The angle Θ is the measure of deviation from the $\langle 111 \rangle$ direction, and the angle φ is the polar angle of the isometric projection of the elementary cell presented in Fig. 5(b).

The dependence of transmission of light on the propagation direction was measured in an opal sample cut parallel to the (111) plane. Transmission spectra of the opal sample impregnated with water for various propagation directions are presented in Fig. 6. In this case, the angle φ was fixed such as to correspond to cross-sections of the Brillouin zone by (ΓLX) (a) and (ΓLK) (b) planes, whereas the angle Θ varied from 0° to 48°. An increase in Θ corresponds to moving away from the $\langle 111 \rangle$ direction. The stop band changes its spectral position, and becomes less pronounced with Θ. This agrees well with the fact that most efficient Bragg reflections in a fcc lattice are those from planes with all odd or all even Miller indices. Other planes participate in higher order reflections at shorter wavelengths. Unfortunately, the spectral region available for investigation was restricted by our experimental setup, and we were unable to perform reliable measurements in cases when the light beam fell on the sample at an acute angle. Therefore, only the ''red'' wing of the stop band can be observed in Fig. 6 for Θ values greater than 30°.

The angular dependences obtained are summarized in Fig. 7 in the form of polar diagrams in coordinates $(\Delta\lambda, \varphi)$ (a) and (Θ, φ) (b), where $\Delta\lambda$ is the difference between the position of the dip measured for propagation along the $\langle 111 \rangle$ direction ($\Theta = 0°$) and the dip position measured for propagation at various φ angles at a fixed $\Theta \neq 0$. Figure 7(a) presents relative spectral positions $\Delta\lambda$ of the dip measured for various directions $0 < \varphi < 360°$ at $\Theta = 20°$ (curve 1) and

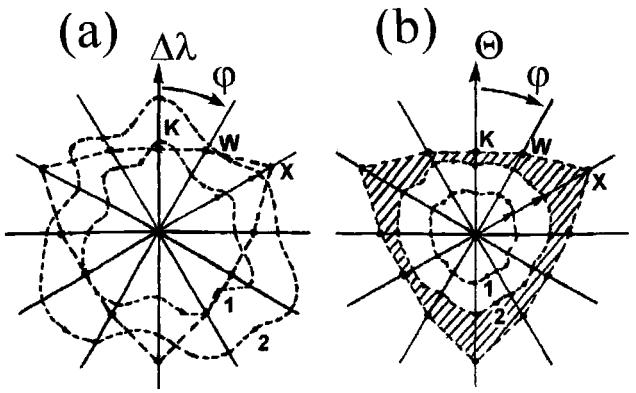

FIG. 7. (a) Stop band shift $\Delta\lambda$ relatively light propagation along $\langle 111\rangle$ direction for $0 \leqslant \varphi \leqslant 360°$ at $\Theta = 20°$ (curve 1) and $\Theta = 30°$ (curve 2). (b) Θ angles which correspond to the stop band spectral position at 530 (curve 1) and 500 nm (curve 2) for $0 \leqslant \varphi \leqslant 360°$.

$\Theta = 30°$ (curve 2). Figure 7(b) shows Θ angles corresponding to the same position of the transmission dip [530 nm (curve 1) and 500 nm (curve 2)]. From these diagrams the presence of a third-order axial symmetry is evident. A certain violation of symmetry may be due to the imperfection of the crystals. Curve 2 in Fig. 7(b) bounds the area of directions along which a sharp decrease in light transmission was observed.

We investigated the fluorescence of dye molecules embedded in artificial opal samples with a photonic stop band situated within and outside the region of dye fluorescence. The samples were prepared by impregnating the opal with an ethanol solution of Rhodamine 6G (R6G). Upon evaporation of the solvent, experiments on dry samples were carried out. Fluorescence was excited by radiation of a nitrogen laser ($\lambda_{ex} = 337.1$ nm). We measured fluorescence spectra of the dye in opal samples at various observation angles α with respect to the normal to the sample surface. Fluorescence spectra $S_\alpha(\lambda)$ of R6G in an opal sample, with the photonic stop band situated within the region of the dye fluorescence recorded at various observation angles α and normalized such as to have approximately equal intensities at the wings, are presented in Fig. 8(a). For comparison, the fluorescence spectrum of R6G in an opal sample with the photonic stop band located outside the spectral region of the dye fluorescence is presented in the same figure by squares. For this sample, the shape of the fluorescence spectrum should not ''sense'' the presence of the photonic stop band, and can therefore be referred to here as a ''vacuum'' spectrum; therefore, we denoted it by $S_{vac}(\lambda)$. It is evident from Fig. 8(a) that fluorescence spectra change their shapes substantially with the observation angle. In order to make the picture more evident, we plotted $S_\alpha(\lambda)/S_{vac}(\lambda)$ ratios for several observation angles [Fig. 8(b)]. As is clear from the figure, the spectral position and shape of the dip in the relative fluorescence intensity depend on the observation angle, which agrees well with the above-presented results on optical transmission of opal samples. However, the contrast of the dip is not so high as in optical transmission experiments (cf. Fig. 3). In our opinion, this can be explained by the fact that the opal is a highly scattering medium, and therefore dye molecules situated in the vicinity of the surface of the sample, and thus not

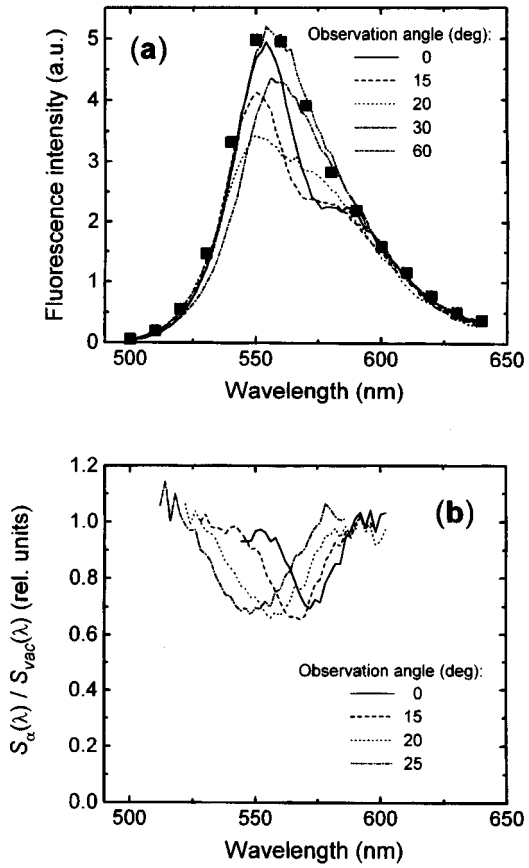

FIG. 8. Fluorescence spectra of dye molecules (Rhodamine 6G) embedded into the opal. Panel (a) shows spectra measured at various observation angles with respect to the normal to the sample surface. Squares represent the emission spectrum of the same dye embedded in the sample with the stop band located outside the fluorescence emission range (''vacuum'' spectrum). Panel (b) contains the same spectra divided by the latter one.

affected by the 3D structure of the opal, contribute more substantially to the total fluorescence intensity. The effect of the photonic pseudogap in the artificial opal on the fluorescence lifetime of dye molecules embedded in the matrix is currently being investigated [19].

III. THEORY

The appearance of localized states and the formation of dips in the transmission spectrum of photonic crystals becomes possible due to the interference of waves which experience multiple scattering by a partially ordered system of mesoscopic particles. In order to calculate the optical characteristics of such a system, a technique based on statistical multiple wave scattering theory can be used. This technique is widely used in studies of the interaction of electromagnetic radiation with randomly inhomogeneous media (see, e.g., Ref. [20]). We used the technique [21] to calculate coherent transmission and reflection of a multilayer scattering medium consisting of periodically alternating homogeneous and close-packed disperse layers. When the thickness of homogeneous layers approaches zero, the structure of such a system becomes similar to that of photonic crystals, if packing of particles in the disperse monolayers is extremely high. In

this section we consider basic principles of the calculation technique, and perform calculations for structures similar to opal matrices and their replicas.

In order to describe spectral features of transmission and reflection of a multilayer scattering medium consisting of a system of correlated scatterers, one should take into account interference cooperative effects, namely, coherent rescattering on particles and interference of the scattered waves. Cooperative effects in a single monolayer are usually considered within the quasicrystalline approximation [22,23]. In a multilayer system, not only the incident radiation field and the fields scattered by other particles of the same monolayer contribute to the effective field for a given particle, but fields from particles of other layers also do.

This is the main difference of the multilayer system as compared to a single monolayer. Based on the assumption of the statistical independence of the individual monolayers, it is possible to find first the scattering amplitude of a single monolayer by taking into account multiple rescattering on particles within the layer, and then to account for the reirradiation of different monolayers of the sample under consideration.

We suppose that all the layers are parallel to each other and equally spaced. Let us consider a wave vector $\mathbf{k}$ of the incident plane monochromatic wave to be normal to the plane of the monolayers and parallel to the unit vector $\mathbf{z_0}$, giving the z-axis direction. In order to describe the coherent field of a single monolayer we use the scattering amplitudes $\mathbf{F}^{\pm}\equiv\mathbf{F}(\pm\mathbf{z}_0)$ within the quasicrystalline approximation in the form

$$\mathbf{F}^{+}=-\mathbf{e}\frac{\pi}{k^2}\sum_l \rho(2l+1)(c_l+d_l), \tag{1}$$

$$\mathbf{F}^{-}=-\mathbf{e}\frac{\pi}{k^2}\sum_l \rho(-1)^l(2l+1)(c_l-d_l). \tag{2}$$

In Eqs. (1) and (2) the plus and minus signs correspond to the transmitted and reflected waves, respectively. The coefficients c_l and d_l satisfy the expressions

$$c_l=a_l+a_l\sum_l \rho[P_{ll'}c_{l'}+Q_{ll'}d_{l'}], \tag{3}$$

$$d_l=b_l+b_l\sum_l \rho[P_{ll'}d_{l'}+Q_{ll'}c_{l'}], \tag{4}$$

where a_l and b_l are the Mie coefficients, ρ is the surface concentration of particles, and $P_{ll'}$ and $Q_{ll'}$ are the coefficients that take into account coherent irradiation of the particles within a monolayer. Explicit expressions for $P_{ll'}$ and $Q_{ll'}$ are rather complicated, and can be found in Refs. [22,23]. Here we just note that these expressions include the radial distribution function $g(r)$ which accounts for correlation in the arrangement of particles. This function can be calculated by using a model of solid spheres. For a close-packed system of particles the $g(r)$ function has sharply pronounced maxima for r values corresponding to the most probable distances between particles. This behavior of $g(r)$ reflects the short-range order in the system. For the closest packing of particles the symmetry of their arrangement is close to the hexagonal one.

The coherent field of a multilayer medium consisting of monolayers can be written as follows:

$$\langle\mathbf{E}^{+}(\mathbf{z})\rangle=\exp(ik|z|)\left[\mathbf{e}+\sum_{j=1}^{N}\mathbf{G}_j^{+}\right], \tag{5}$$

$$\langle\mathbf{E}^{-}(\mathbf{z})\rangle=\exp(ik|z|)\sum_{j=1}^{N}\mathbf{G}_j^{-}\exp[(j-1)2ikl_m], \tag{6}$$

with $\mathbf{e}$ being a unit polarization vector of the incident wave; $G_j^{\pm}\equiv G_j(\pm\mathbf{z}_0)$ are the forward and backward scattering amplitudes of the jth monolayer in the presence of other monolayers, and l_m is the interlayer spacing. We use the method of self-consistent field which provides consideration for irradiation between the monolayers to evaluate $\mathbf{G}_j^{\pm}$. In this case $\mathbf{G}_j^{\pm}$ satisfies the expressions

$$\mathbf{G}_m^{+}=F^{+}+F^{+}\sum_{j-1}^{m-1}\mathbf{G}_j^{+}+F^{-}\sum_{j=m+1}^{N}\mathbf{G}_j^{-}\exp[(j-m)2ikl_m], \tag{7}$$

$$\mathbf{G}_m^{-}=F^{-}+F^{-}\sum_{j-1}^{m-1}\mathbf{G}_j^{+}+F^{+}\times\sum_{j=m+1}^{N}\mathbf{G}_j^{-}\exp[(j-m)2ikl_m]. \tag{8}$$

The sums in Eqs. (5) and (6) describe coherent irradiation that the mth layer experiences from other layers. In order to evaluate the coherent transmission coefficient $T^k=|\langle\mathbf{E}^{+}(\mathbf{z})\rangle|^2$ and the coherent reflection coefficient $R^k=|\langle\mathbf{E}^{-}(\mathbf{z})\rangle|^2$ one should solve a system of equations (7,8) with respect to $G_m^{\pm}$, and then substitute the solution into Eqs. (5) and (6).

Numerical calculations have been carried out for a layered system consisting of close-packed monolayers of spherical particles with hollow voids and with voids filled with another material with different refraction index. The refraction index of the spheres was taken to be equal to $n_{\text{eff}}=1.26$, which is close to the effective refraction index of silica clusters in the artificial opals. The density of the particle arrangement within a given monolayer was close to maximum (the overlapping factor $\eta=\rho\pi d^2/4=0.6$). The interlayer spacing, defined as the distance between two planes connecting centers of particles in two neighboring monolayers, was taken to be equal to the particle diameter d.

The coherent transmission and reflection of the system are presented in Fig. 9 as functions of the dimensionless parameter $x=\pi d/\lambda$ for a set of numbers N of monolayers in the system. It should be noted that we can introduce the parameter x since $l_m=d$ in the system under consideration. It is evident from the figure that for $N\geqslant 2$ a dip in the transmission spectrum and the corresponding maximum in the reflection spectrum appear, which grow with increasing N. The spectral position of the dip for $d=0.2$ μm and $x=1.43$ corresponds to the wavelength $\lambda\approx 440$ nm. For $d=0.3$ μm we

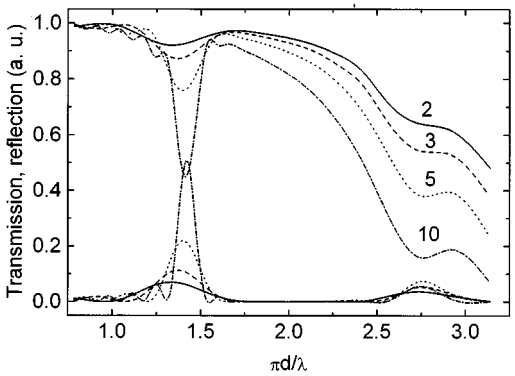

FIG. 9. Optical transmission and reflection spectra for a set of sequentional layers consisting of close-packed spheres with the cubic symmetry. Numbers at the curves indicate the number of the layers. The refraction index of spheres vs voids is 1.26.

obtained $\lambda \approx 660$ nm. Therefore, an increase in particle dimensions (which is equivalent in the case of the opals to an increase in the interlayer spacing) results in the long-wavelength shift and broadening of the dip.

Transmission spectra for systems with filled voids for $d=0.2$ μm and $N=300$ are shown in Fig. 10. The dip shifts toward the long-wavelength region and deepens with the increase in the refraction index n_{fil} of the material embedded in voids. The calculated dependence of the position of the dip on the refraction index of the filler for structures similar to that examined experimentally in Sec. II, is presented in Fig. 4 along with the experimentally measured dependence. It is evident that the calculated and experimentally measured dependences of the dip position on the refraction index of the filler are qualitatively similar. The theory yields the faster growth of the position of the dip with n_{fil}. The possible reason for this discrepancy can be connected with the partial impregnation of silica globules by the filler, resulting in a change in the effective refraction index of the globules.

IV. SUMMARY AND CONCLUSIONS

In summary, we have demonstrated the formation of a photonic frequency stop band in a three-dimensional dielectric lattice consisting of two sublattices of the refractive media with small dissipative losses. Numerical simulations based on the quasicrystalline approximation show reasonable agreement with experimental results. The results obtained can be interpreted in terms of a renormalization of the photon density of states, and the formation of a photonic pseudogap. Along with the findings reported by other authors [10–12,24], this result is a step toward fabrication of a photonic crystal actually exhibiting a forbidden gap in the photon density of states with a number of challenging consequences in the light-matter interaction. Further progress towards solid-state photonic crystals can be achieved by an enhancement of the relative refraction index up to values $n \approx 2$ and higher. One of the possible ways is, e.g., an impregnation of the opals by sol-gel emulsions that experience solidification after filling to form a solid-state lattice with a large n value. Such a possibility has been recently demonstrated for several other porous media [25,26]. Another way is to impregnate opals with polycrystalline semiconductors.

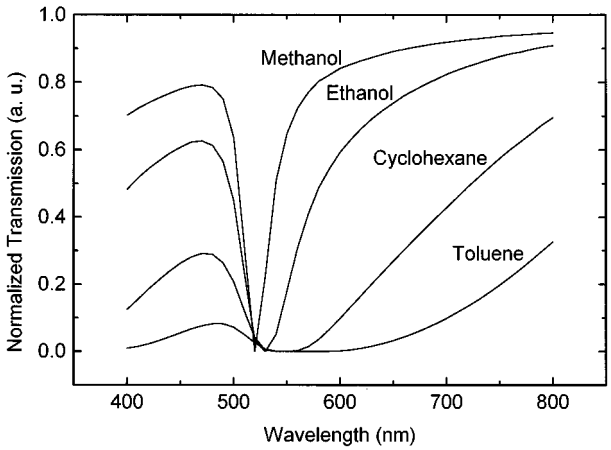

FIG. 10. Calculated normalized transmission spectra of the multilayer close-packed system consisting of spherical particles. The particle diameter is $d=0.2\mu$m, the particle refraction index is $n_{\mathrm{eff}}=1.26$, and the number of the layers is $N=300$. The refractive index of the medium embedded in the interparticle voids is $n_{\mathrm{fil}}=1.0$ (1), 1.328 (2), 1.361 (3), 1.426 (4), and 1.497 (5).

The first results in this field have recently been reported by Astratov *et al.* [27].

As the next step, embedding of light-absorbing and emitting species like rare-earth ions, organic molecules, and semiconductor quantum dots will provide experimenters with an opportunity to test basic effects that are of great theoretical and practical importance. A number of basic phenomena inherent in photonic crystals have been discussed in the literature [1,2,4–6].

In addition, we wish to outline the effects promoted by the interplay of intrinsic properties of species embedded in the photonic crystal, and the enhanced sensitivity of properties of the crystal to small deviations of material parameters: (i) intensity-dependent spectral bandpass, stop band, and cutoff features due to intensity-dependent refraction and absorption index of the filler, e.g., semiconductor quantum dots; and (ii) electric-field-dependent transmission, reflection, and deflection due to electric modulation of the refraction index of the filler. The former provides an effective way of controlling light by light, whereas the latter may be used in electro-optical devices. Both effects will occur not only in the case of the actual photonic band gap, but also in the case of a pseudogap. The aforementioned issues will be the subject of our forthcoming papers.

Taking into account the previously reported results on unique interference-based electronic properties of the 3D mesoscopic arrays made from opals (Josephson media [28,29], a 3D array of tunnel junctions [30], or thermionic converters [26]) we may conclude that opal matrices look very promising for creating advanced electronic, electro-optical, and optical circuitry.

ACKNOWLEDGMENTS

Stimulating discussions with Professor S. Ya. Kilin and Professor A. N. Rubinov are acknowledged. The work was supported by the Foundation for Basic Research of the Republic of Belarus, and in part by the International Soros Science Educational Program.

[1] E. Yablonovitch, Phys. Rev. Lett. **58**, 2059 (1987).
[2] S. John, Phys. Rev. Lett. **58**, 2486 (1987).
[3] *Photonic Band Gap Materials*, Special Issue of J. Opt. Soc. Am. B **10** (2), (1993); *Photonic Band Structures*, Special Issue of J. Mod. Opt. **41** (2), (1994).
[4] S. Ya. Kilin and D. S. Mogilevtsev, Opt. Spektrosk. **74** 974 (1993) [Opt. Spectrosc. **74**, 579 (1993)].
[5] G. Kweon and N. M. Lawandy, Opt. Commun. **118**, 388 (1995).
[6] S. John and Tran Quang, Phys. Rev. Lett. **74**, 3419 (1995).
[7] E. Yablonovitch and T. J. Gmitter, Phys. Rev. Lett. **63**, 1950 (1989).
[8] E. Özbay, G. Tuttle, M. Sigalas, C. M. Soukoulis, and K. M. Ho, Phys. Rev. B **51**, 13 961 (1995).
[9] K. Tanaka, T. Nakamura, W. Takamatsu, M. Yamanishi, Y. Lee, and T. Ishihara, Phys. Rev. Lett. **74**, 3380 (1995).
[10] N. M. Lawandy, S. A. Johnston, and Jordi Martorell, Opt. Commun. **65**, 425 (1988).
[11] J. Martorell, and N. M. Lawandy, Phys. Rev. Lett. **65**, 1877 (1990).
[12] İ. İ. Tarhan, M. P. Zinkin, and G. H. Watson, Opt. Lett. **20**, 1571 (1995).
[13] J. V. Sanders, Acta Crystallogr. A **24**, 427 (1968).
[14] V. N. Bogomolov, D. A. Kurdyukov, A. V. Prokof'ev, and S. M. Samoilovich, Pis'ma Zh. Exp. Teor. Fiz. **63**, 496 (1996) [JETP Lett. **63**, 520 (1996)].
[15] V. N. Bogomolov, A. V. Prokof'ev, and S. M. Samoilovich, Fiz. Tekh. Poluprovodn. (to be published) [Sov. Phys. Semicond. (to be published)].
[16] V. N. Bogomolov, L. S. Parfen'eva, A. V. Prokof'ev, I. A. Smirnov, S. M. Samoilovich, A. Jezowskii, J. Mucha, and H. Miserek, Fiz. Tverd. Tela (Leningrad) **37**, 3411 (1995) [Sov. Phys. Solid State **37**, 1874 (1995)].
[17] V. N. Bogomolov and T. M. Pavlova, Fiz. Tekh. Poluprovodn. **29**, 826 (1995) [Sov. Phys Semicond. **29**, 428 (1995)].
[18] C. Reichardt, *Solvents and Solvent Effects in Organic Chemistry*, 2nd ed. (VCH, Weinheim, 1988).
[19] E. P. Petrov, A. N. Rubinov, V. N. Bogomolov, A. V. Prokofiev, S. M. Samoilovich, A. M. Kapitonov, I. N. Germanenko, and S. V. Gaponenko (unpublished).
[20] A. Ishimary, *Wave Propagation and Scattering in Random Media* (Academic, New York, 1978).
[21] A. N. Ponyavina and N. I. Silvanovich, Opt. Spektrosk. **76**, 648 (1994) [Opt. Spectrosc. **76**, 581 (1994)].
[22] A. N. Ponyavina and N. I. Silvanovich, Zh. Prikl. Spektrosk. **53**, 299 (1990) [J. Appl. Spectrosc. **53**, 884 (1990)].
[23] K. M. Hong, J. Opt. Soc. Am. **70**, 821 (1980).
[24] J. Martorell and N. M. Lawandy, Opt. Commun. **78**, 169 (1990).
[25] A. M. Dorofeev, N. V. Gaponenko, V. P. Bondarenko, E. E. Bachilo, N. M. Kazuchits, A. A. Leshok, G. N. Troyanova, N. N. Vorosov, V. E. Borisenko, H. Gnaser, W. Bock, P. Becker, and H. Oechsner, J. Appl. Phys. **77**, 2679 (1995).
[26] V. N. Bogomolov, D. A. Kurdyukov, A. V. Prokofiev, Yu. A. Ravich, S. M. Samoilovich, and L. A. Samoilovich, Phys. Low-Dim. Struct. **11**, 63 (1994).
[27] V. N. Astratov, V. N. Bogomolov, A. A. Kaplyanskii, A. V. Prokofiev, L. A. Samoilovich, S. M. Samoilovich, and Yu. A. Vlasov, Nuovo Cimento D **17**, 1349 (1995).
[28] V. N. Bogomolov, V. V. Zhuravlev, A. I. Zadorozhnii, E. V. Kolla, and Yu. A. Kumzerov, Pis'ma Zh. Eksp. Teor. Fiz. **36**, 298 (1982) [JETP Lett. **36**, 365 (1982)].
[29] V. N. Bogomolov, Y. A. Kumzerov, S. G. Romanov, and V. V. Zhuravlev, Physica C **208**, 371 (1993).
[30] V. N. Bogomolov, S. A. Ktitorov, D. A. Kurdyukov, A. V. Prokof'ev, S. M. Samoilovich, and D. V. Smirnov, Pis'ma Zh. Eksp. Teor. Fiz. **61**, 738 (1995) [JETP Lett. **61**, 753 (1995)].